EXPERIMENTAL STUDY ON HYPERSONIC HEATING CHARACTERISTICS OF CAVITY WAKE FLOW

Koichi HOZUMI*, Tadao KOYAMA, Noriaki HIRABAYASHI****
***Foundation for Promotion of Japan Aerospace Technology (JAST)**
****Japan Aerospace Exploration Agency (JAXA)**

Keywords: *cavity wake flow, hypersonic, heat transfer, correlation, peak heating*

Abstract

In order to investigate cavity wake heating characteristics, a series of tests by parametrically changing cavity size were conducted. Two-dimensional heat flux distribution around cavities on flat plate models was measured by IR camera at a Mach number of 10 and angle of attack of 35 degrees. A correlation study was attempted assuming that the magnitude of the wake heating depends on the resonant frequency in the cavity. The study showed that the cavity peak, far wake and the inside the cavity heating, are correlated well with the combined parameter of the Strouhal number of the cavity resonant frequency and length to depth ratio; $Str/(L/D)^2$, if the corrections of the effect of the boundary layer thickness at the leading edge of cavity are made for the heating. The results indicate a single correlation line for the wake peak heating and two clearly distinguishable laminar and turbulent correlation lines for far wake heating. These result show that shear layer instability oscillation dominantly affect the amount of the heat transfer and the transition within the cavity and along the cavity wake flow.

1 Introduction

Estimation of local heat flux increase caused by distortion on the surface, such as local severe peak heating and strong heating wake flow associated with dent or cavity, is essential for the aerothermal design of hypersonic winged vehicles.

In subsonic to supersonic flow region, many studies on cavity characteristics have been conducted because of their practical importance relating to the resonance drag and noise reduction in flight [1, 2, 3]. However, in hypersonic flow region, in spite of its importance to predict heating increase, caused by such as the damage of the thermal protection tile, not so many studies on the heating characteristics have been conducted.

In our preliminary tests, strong heating wakes occurred in complicated manner, depending on the cavity geometry and free stream conditions. Therefore, in order to investigate cavity geometry effect on the heating and transition characteristics, we performed a parametric study, assuming that the shear layer instability plays dominant roll on the heating and transition characteristics of the cavity wake flow.

2 Description of Experiment

2.1 Experimental Setup

For cavities on windward side of flat plates at an angle of attack α = 35 deg, heat flux measurement tests were conducted in the JAXA 1.27m hypersonic wind tunnel at a Mach number 10, stagnation pressure P_0=2.5 and 1.0MPa, stagnation temperature T_0 = 640 - 740 °C. These test conditions, which give the free stream Reynolds number Re_∞ = 0.65 - 1.5×10^6/m, were selected as to make the flow without cavity laminar, but to make flow with cavity on the edge of the onset of the boundary layer transition at the downstream of the cavity.

The flat plate model of 470mm length and 200mm width with interchangeable cavities was used, as shown in Fig.1. The location of the leading edge of cavity was fixed at X_{LE} =

131mm from the leading-edge of the model for all test cases. For the material at the region of the heat transfer measurement, a polyimide plastic (Vespel®) was used. And for the leading-edge of the model two stainless steel noses of Nose 1 and Nose 2 with nose radius *Rn* = 0.3mm and 3.0mm, respectively were used.

Cavity geometries used in the test: cavity length L, cavity depth *D* and cavity width *W* and the observed flow conditions at cavity far wake region: laminar LAM and turbulent Turb, are summarized in Table 1.

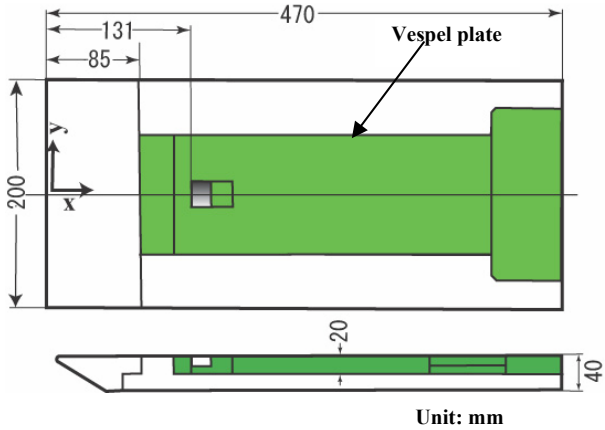

Fig.1 Model Geometry

Table 1 Tested Cavity Geometries

L/D	L	D	W	Wake flow transition			
				Nose 1		Nose 2	
				P_0=1.0	P_0=2.5	P_0=1.0	P_0=2.5
16	40	2.5	20	-	Turb	Lam	-
8	40	5.0	20	Lam	Turb	Lam	Turb
	20	2.5	20	-	Lam	-	Turb
6	15	2.5	15	-	Lam	-	-
4	40	10	20	Turb	Turb	Turb	-
	20	5.0	20	Lam	Turb	Lam	Turb
	10	2.5	10	-	Lam	Lam	Turb
3.2	40	12.5	20	-	Turb	Turb	-
3.0	15	5.0	15	Lam	Lam	Lam	-
2	20	10	20	Lam	Turb	Turb	-
	10	5.0	10	-	Turb	-	-
1.6	20	12.5	20	Lam	Turb	-	-
1.5	15	10	15	Lam	Turb	Lam	-
1.17	11.7	10	20	-	Lam	Lam	Turb
1.0	10	10	10	-	Turb	-	-

2.2 Heat Transfer Measurement Procedure

The model was outside of the main flow before running the tunnel and after 20 seconds from the start of the run, when the fully constant stagnation temperature was attained, the model was injected into the main stream by high speed injection system. The images of the model were obtained using two infra-red (IR) cameras that have 12 bit temperature resolution (AGEMA-900LW). Lense of view angle of 20 was used for the whole image of the model and lense of view angle of 5 degree was used to take the close up image for the calculation of heat flux.

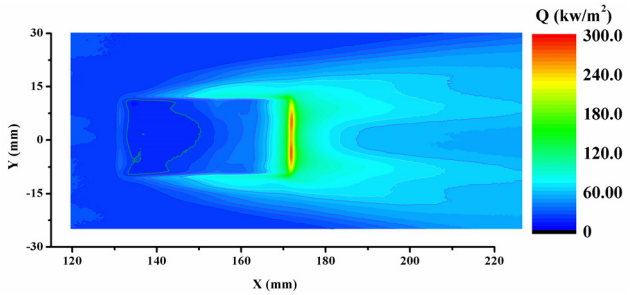

a) Strong heating case (L=40mm, D=10mm)
(M_∞=9.59, P_0=2.5Mpa, T_0=700°C)

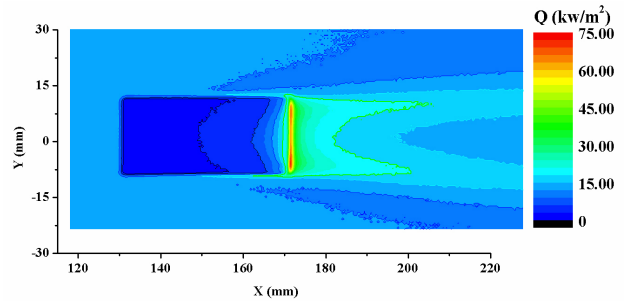

b) Weak heating case (L=40mm, D=5mm)
(M_∞=9.46, P_0=1.0Mpa, T_0=700°C)

Fig.2 IR Images for Cavity Wake Heating

Heat transfer coefficients were derived by the JAXA heat transfer measurement system based on the Jones-Hunt method, whose accuracy was fully examined through series of tests [4]. The measured data from the close up image by 5 degree lens for the sharp peak heating is accurate enough although the heating area is very close to the measurement limit which depends on the limit of the pixel resolution of the IR camera.

Schlieren photographs were also taken to supplement the IR image data. However, the shock and expansion waves around the cavity were not visible.

3 Experimental Results

3.1 IR Image of Heat Transfer Distribution

Examples of the obtained IR thermography image (iso-heat flux image) are shown in Fig.2 for a) strong heating and b) weak heating. A sharp peak heating at the immediate downstream of cavity trailing edge and the succeeding hot heating wake were observed. The magnitude of heating level showed complicated dependency on the cavity geometry and flow conditions.

3.2 Centerline Heat Transfer Distribution

To compare the magnitude of heat flux q in different flow conditions, a modified Stanton number St_m was used,

$$St_m = St/[Vp(1.0-T_w/T_0)] \qquad (1)$$

where $St = h/\rho_\infty U_\infty$ is Stanton number, $h = q/(CpT_0-CpT_w)$ is heat transfer coefficient, $Vp = M_\infty/\sqrt{Re_\infty}$ is viscous parameter. The suffix ∞, 0, and w indicate the values at free stream, stagnation, and wall conditions, respectively.

For the cavity wake flow that follows downstream of the peak heating region, three heating levels of cavity wake flow were observed. Fig.3 shows a plot of centerline heat transfer distribution of Stm for the strong and weak heating wakes. The strong peak heating, observed at immediately downstream of the cavity trailing-edge, has the magnitude of 3-7 times larger than that of cavity free flat plate flow. Fig.4 shows examples of the case of middle heating level. Most cavity wake flows downstream of strong peak heating become turbulent and most wake flows after weak peak heating are laminar. However, the wake flows after middle magnitude peak heating become either laminar or turbulent flow.

Judging from these heat transfer distribution we assumed that the wake flow is turbulent when the heating level at far wake region is larger than an assumed turbulent heating level, i.e., St_m >650 at X = 300 mm. In Fig.6, and in all figures after Fig.10, we used the solid and the open symbols for the test case in which the far wake flows are turbulent and laminar, respectively.

The heat transfer distribution without cavity shows laminar flat plate heat transfer distribution. For the case of the Nose 2 model at P_0=2.5MPa, because of the nose bluntness effect, the earlier transition of boundary layer occurred from near cavity trailing-edge position (approximately X = 140mm) showing slight increase of heating level. However, this onset of transition seems to give little effect for the present test results.

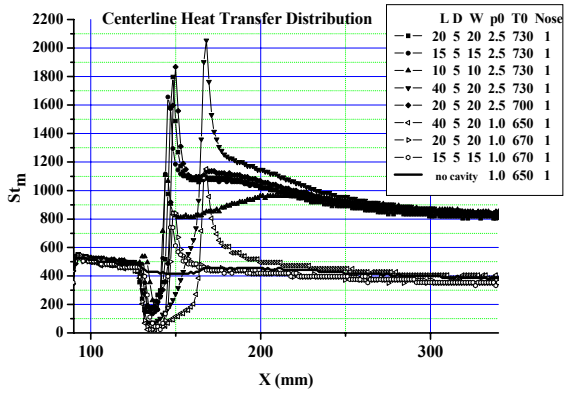

Fig.3 Centerline Heat Transfer Distribution (Strong and Weak Heating Wake)

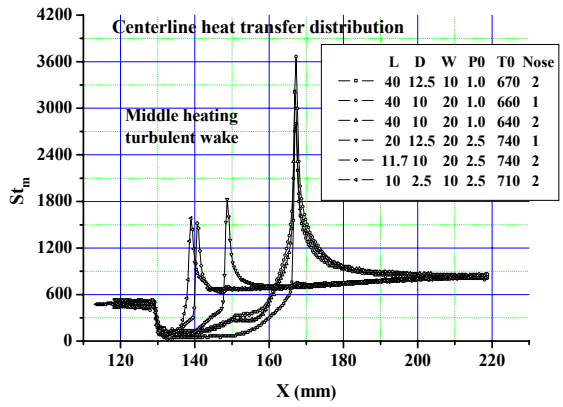

Fig.4 Centerline Heat Transfer Distribution (Middle Heating Wake)

3.3 Heat Transfer Distribution in Cavity

Fig. 5 shows schematic cavity flow structure. The heat transfer distributions at the cavity bottom are shown in Fig. 6 for L/D= 4 cavities. To compare the profiles of the heat transfer

distribution, the distance from leading-edge of cavity X-X_{LE} is normalized by D.

The laminar heat transfer distribution shows almost constant heating level region at the upstream and increasing heating region at the near trailing corner. The turbulent heat transfer distribution shows three heating regions which may show upstream corner vortex flow region, one or two plateau heating region and high heating downstream corner vortex flow region, corresponding to the flow structure inside the cavity as shown in Fig.5.

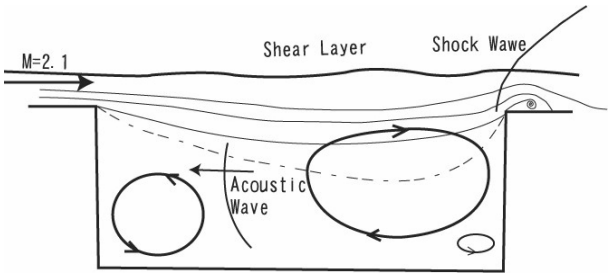

Fig.5 Schematic Cavity Flow Structure

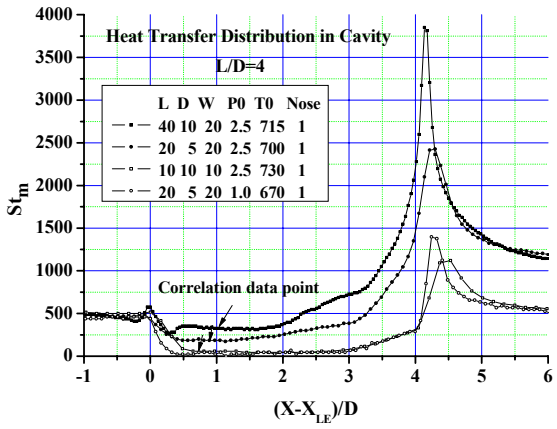

Fig.6 Heat Transfer Distribution
At the Cavity Bottom Surface

3.4 Flows around Peak Heating Region

As shown in the IR heat flux image of Fig 2, heat transfer distribution shows complicated heating patterns around the peak heating region at immediately (1-2mm) downstream of cavity trailing edge. From these heating patterns, the flow structure at immediately downstream of the cavity trailing edge were estimated.

The reference 5 and 6 categorize three-dimensional separated flows into several types. The first owl face type (OF1), the second owl face type (OF2) and simple U-shaped (SU) separations are shown in Fig.7. For most cases in our test, a pair of peak heating was observed, which may show that a tornado-like vortex is induced near the reattachment of the separated shear layer as shown in Fig.7.

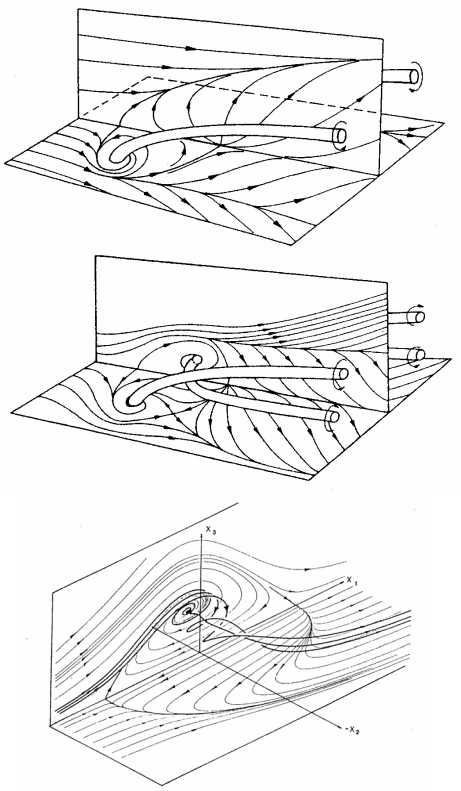

Owl face Type1 (upper), Type2(middle)
Simple U-shaped (lower) separation

Fig.7 Three-Dimensional Separation Categories
(Taken from Ref.5 and 6)

Fig. 8 shows the heat transfer distribution along y axis for the flow with strong heating. Fig.8 a) shows the distributions at 20 positions of every Δx =0.37mm downstream from the peak heating. Fig.8 b) shows the distributions at 10 positions upstream from the peak heating.

Heat transfer distribution of Fig.8 seems to correspond to that of the OF1 type separation flow which shows small outside reattachment peak heating along the outside of wake heating region. For OF1 type separation, this wake

boundary reattachment heating peak creeps up to upstream along the cavity side edge as shown in Fig.8 a) (see also Fig.2 a)).

Fig.9 shows the heat transfer distribution for weak peak heating. This may correspond to OF2 type separation judging from heat transfer distribution dent along the wake boundary that may show outside separation along the OF2 type separation flow. For this spanwise flat heating distribution (without a pair of peak heating), there is other possibility of the case correspond to the simple U-shape type separation.

As can be seen from Fig.8 and 9, the most heating distribution is asymmetry. This may come from the wall stream line pattern asymmetry as shown in Fig. 4 of Ref. 6.

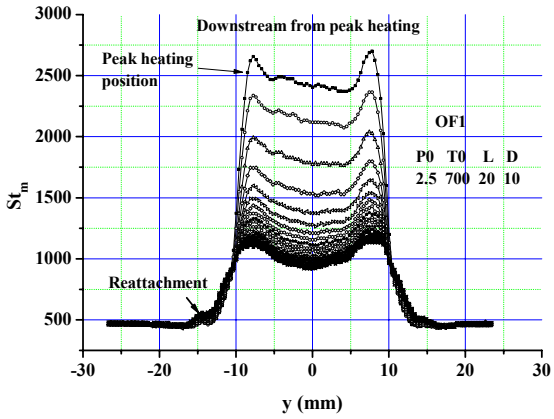

a) Downstream of peak heating

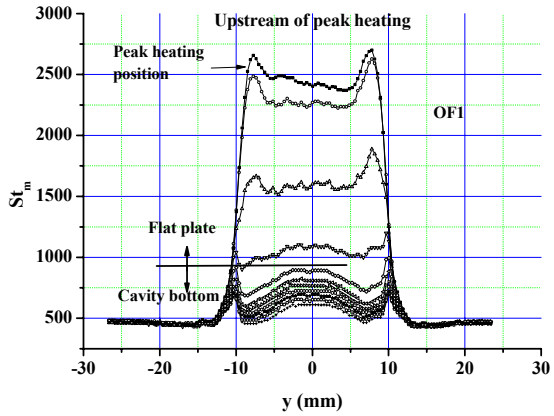

b) Upstream of peak heating

Fig.8 Heat Transfer Distribution around Strong Peak Heating Region

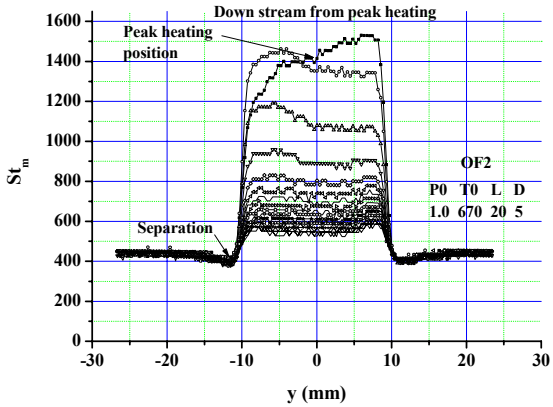

a) Down stream of peak heating

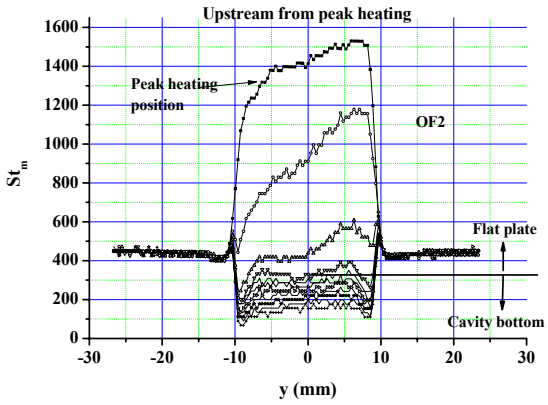

b) Upstream of peak heating

Fig.9 Heat Transfer Distribution around Weak Peak Heating Region

4 Results and Discussion

4.1 Correlation of Wake Peak Heating

The estimation of the cavity heating level was unresolved problem in previous preliminary tests to obtain elementary HOPE design data [7]. We examined the dependency of cavity heating level on the cavity geometry and the flow parameters.

Ref.8 says, through the shear layer instability, the cavity resonance frequency f_{cav} plays important roll for determining the magnitude of pressure oscillation in the open cavity. In this study, we assumed that the shear

layer instability also plays a dominant role in determining the heating characteristics of cavity wake flow, i.e., the cavity wake heating level and cavity transition. In addition to the effect of f_{cav}, we considered that the boundary layer thickness at the leading edge of the cavity δ_0 plays an important roll to determine the shear layer instability amplification. Based on this, an effort to correlate the magnitude of the heat transfer with f_{cav}, the ratio of L/δ_0 and D/δ_0 was made.

In the following correlation study, for flow parameters; velocity u, density ρ, Mach number M and the Reynolds number Re, we used flow conditions behind the oblique shock. For viscosity μ we used the Sutherland viscosity law.

4.1.1 Cavity Resonance Frequency

As we did not measure the cavity oscillation frequency in the present experiments, we examined at first which existing cavity oscillation theory is better to apply to the correlation study. In subsonic to supersonic flow region, to predict the pressure oscillation, many studies were made on cavity resonance mechanism and semi-empirical and analytical formulas have been reported [1, 2, 3 and 9].

Some recent studies show that the simple acoustic resonance plays an important role in the fluid-resonant cavity oscillations. In hypersonic cavity oscillation measurement study [10], comparison of spectral analysis of the fluctuating pressures with the experiment showed that the cavity oscillation frequencies are accurately predicted using the simple closed-box acoustic theory. Supersonic numerical study [9] showed that their numerical results for the peak frequencies at M=1.83 and the L/D=1 and 2 cavities agree with those of standing wave theory.

In the present study, we selected the oscillation frequency of the closed-box acoustics models, as it gave better correlation results than the frequency using the Rossiter's modified formula [2].

The closed-box acoustic modes are modeled as the longitudinal modes in a box of length L filled with air with stagnation speed of sound a_0 [10]. The resonance frequency f_L and the corresponding Strouhal number Str are expressed as

$$f_L = (a_0/2L)n \qquad (2)$$

$$Str=f_L L/u = [1+(r/2)(\gamma-1)M]^{1/2}/(2M)\ n \qquad (3)$$

where n is the mode number of the oscillation and r is recovery factor.

4.1.2 Boundary Layer Thickness δ_0 Effect

Precise studies on the stability characteristics of compressible mixing layer [11, 12, 13] demonstrated that M, the velocity ratio and temperature ratio of the two layers give large influence on the instability amplification. However, in the present study, M_∞ is constant ($M\approx2.1$ for $\alpha=35°$), and because of the almost stagnant flow inside the cavity, the velocity ratio and temperature ratio are also almost constant for the cavity shear layer. Therefore, these parameters do not give detectable change for the instability characteristics. Consequently, we have to be looked for other parameters that will show dominant influence on it.

In the recent numerical cavity wake mode oscillation study [14], it is suggested that the shear layer amplification is a complicated function of M, L/δ_0, D/δ_0 and $Re\delta_0$. In the correlation study using existing experimental heat transfer data [15], the parameter L/δ_0 was used and good correlation results are obtained. Based on these facts, we considered that, in addition to the oscillation frequency, L/δ_0 and D/δ_0 are dominant parameters for the heating of the cavity peak heating.

In this study, δ_0 was estimated from following approximation for flat plate flow [16].

$$\delta_0 /X_{LE}Re_{XLE}^{0.5} =$$

$$Cw^{0.5}[5.0+(0.2+0.9T_w/T_{aw}(\gamma-1)M^2] \qquad (4)$$

where adiabatic wall temperature T_{aw} and C_w are

$$T_{aw}/T=1+Pr^{0.5}(\gamma-1)/2M^2 \qquad (5)$$

$$C_w = (\rho_w\mu_w/\rho\mu). \qquad (6)$$

for a Prandtle number Pr of 0.75 and the air specific ratio γ of 1.4.

The rough dependency check of the present data showed that the magnitude of the peak heating increases mainly with increase of D and with decrease of L/D for constant Reynolds number and D. Considering this dependency comes the δ_0 effect on the heating, St_m is corrected by $[(L/\delta_0)/(D/\delta_0)^2]^n$.

4.1.3 Cavity Peak Heating Correlation Results.

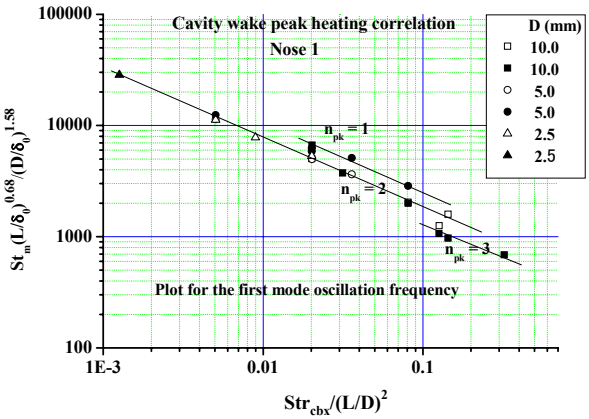

Fg.10 Peak Heating Correlation for the First Closed-box Acoustic Modes (Nose 1)

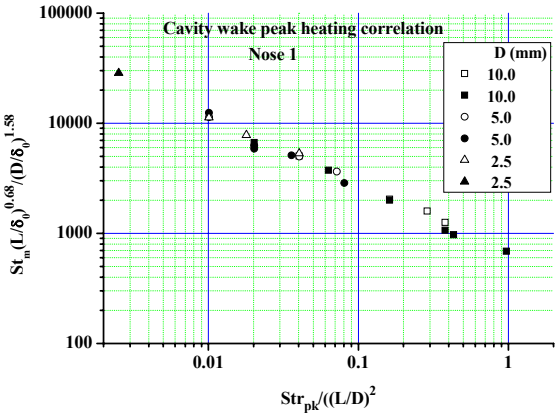

Fig.11 Peak Heating Correlation Based on the Estimated Oscillation f_{pk} (Nose 1)

Fig. 10 shows the correlation results of cavity wake peak heating for the Nose 1 model; $St_m(L/\delta_0)^{0.68}/(D/\delta_0)^{1.58}$ versus $Str_{cbx}/(L/D)^2$, where the first mode of oscillation frequency based on the closed-box formula f_{cbx} is used for the Strouhal number Str_{cbx} $(=f_{cbx}L/u)$. The modified Stanton number St_m corrected by the effect of L/δ_0 and D/δ_0 showed multi-correlation lines, which depend on the first to 3rd frequency mode. Based on this, we estimated the frequency mode number n_{pk} for each data, and defined new Strouhal number Str_{pk} by multiplying n_{pk} to Str_{cbx} (i.e., $f_{pk}=n_{pk}f_{cbx}$, $Str_{pk}=n_{pk}Str_{cbx}$). Fig.10 is re-depicted for the Strouhal number Str_{pk} in Fig.11.

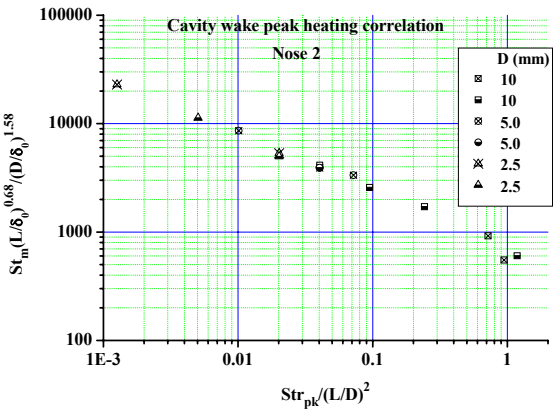

Fig.12 Peak Heating Correlation for the Estimated Oscillation f_{pk} (Nose 2)

Fig.12 shows the correlation results for the Nose 2 model. Both Fig.11 and 12 shows a single correlation line for the magnitude of the wake peak heating, whether the flow is laminar or turbulent.

This may show the fact that the oscillating amplitude level at peak heating region, which come from the shear layer instability oscillation, follow the same character for all cases of cavity geometry in the present test. Consequently the impinging flow at the peak heating region has the same character of oscillation amplitude.

4.2 Correlation of Far Wake Heating

The induced vortex at the immediate downstream of cavity trailing edge will be imbedded in the boundary layer and develop as the wake flow with a pair of vortex. As it flows downstream, the heating rate (St_m) approaches constant level with flat y direction distribution as can be seen from Fig.3, Fig.8 a) and Fig.9 a). These tendencies may show the diffuse away of the vortex core.

Assuming that the magnitude of the heating at the far wake region is also related to

the oscillation frequency of the peak heating region, correlation using Str_{pk} (which is used in Fig.11, 12) are made for St_m at X = 215 mm. And from the obtained multi correlation lines of different oscillation mode for f_{pk}, we determined the oscillation frequency mode number at far wake region n_{wk} (i.e., $f_{wk}=n_{wk}f_{pk}$.).

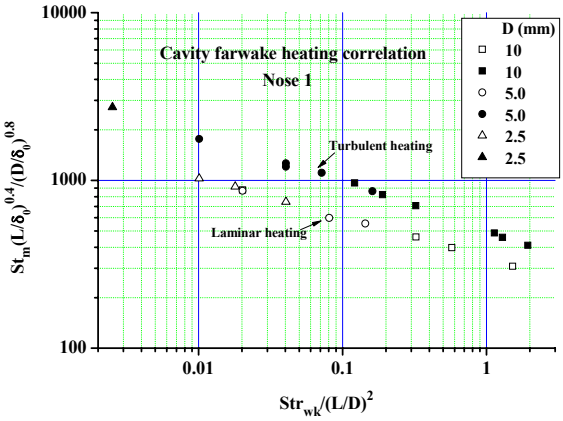

Fig.13 Far Wake Heating Correlation with the Estimated Str_{wk} (Nose 1)

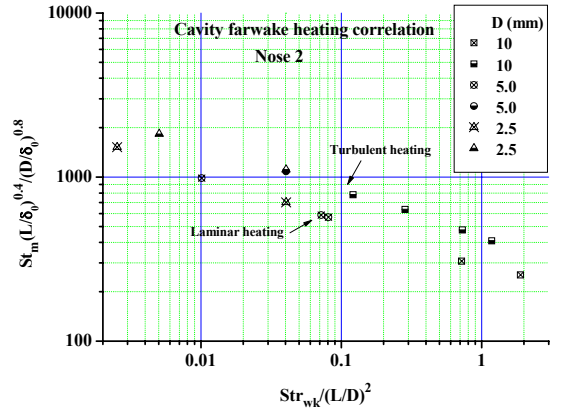

Fig.14 Far Wake Heating Correlation with the Estimated Str_{wk} (Nose 2)

Fig.13 shows the correlation results of the far wake heating for Nos1 and Fig.14 shows the results for Nose 2. Str_{wk} is the estimated Strouhal number which corresponds to the determined far wake oscillation frequency f_{wk}.

For strong, middle and weak heating level of far wake heating data as shown in Fig.3 and 4, good two correlation lines, which may correspond to the far wake laminar and turbulent heating, are obtained. The L/δ_0 and D/δ_0 correction is smaller than that in the cavity peak heating correlation and the estimated f_{wk} is 1 - 3 times higher than the peak heating frequency f_{pk}. These results may show that the instability in the wake develops following different mechanism compared with the instability at peak heating region which may be directly related to the cavity shear layer instability.

4.3 Correlation of Cavity Bottom Heating

4.3.1 Correlation result

It is interesting to know the relation between the peak heating, the far wake heating and the heating within the cavity.

In the same way as the determination of n_{wk} and f_{wk} for cavity far wake heating, oscillation mode number for cavity bottom heating n_{cav}, oscillation frequency for bottom heating f_{cav} (= $n_{cav}f_{pk}$) and the corresponding Strouhal number Str_{cav} were determined. Higher mode of oscillation and larger correction of the effect of L/δ_0 and D/δ_0 are observed compared with those for cavity peak heating. For correlation of cavity bottom heating, St_m of the plateau bottom heating at upstream region is selected for the correlation as shown in Fig. 6.

Cavity bottom heating correlation for Nose 1 model, shown in Fig.15, indicates two correlation lines for laminar and turbulent heating. Solid symbol in the laminar and open symbol in the turbulent correlation lines should be laminar and turbulent in the cavity flow, respectively.

The correlation for the Nose 2 model, shown in Fig. 16, indicates a single correlation line for both laminar and turbulent cavity flow. This difference between the Nose 1 and Nose 2 correlation cases may come from the fact that difference of shear layer profile caused by the nose bluntness effect. In the Nose 2 case, the state of laminar or turbulent flow are not clearly distinguishable from St_m level although there is some consistency between the heating level in the cavity bottom heating and the far wake flow condition.

In Fig.16, there are a few cases that deviate from the correlation line. Further effort will be necessary to clarify the reason for this low level heating.

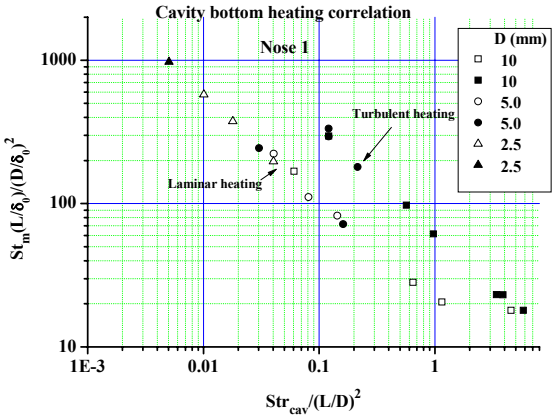

Fig.15 Correlation of Cavity Bottom Heating with the Estimated Str_{cav} (Nose 1)

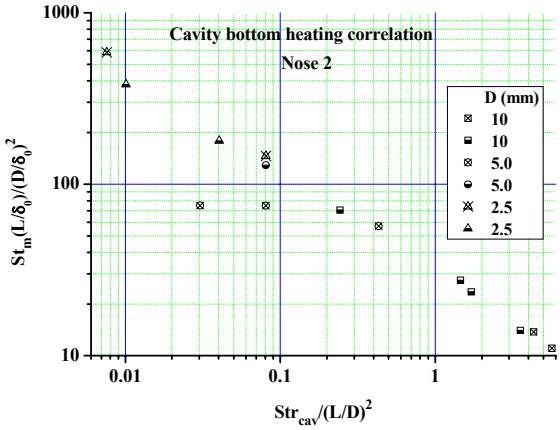

Fig.16 Correlation of Cavity Bottom Heating with the Estimated Str_{cav} (Nose 2)

4.3.2 Cavity wake transition boundary

It was the initial question when we started the present study whether the unexpected wake transition is triggered by shear layer instability or cavity flow instability.

Hankey & Shang [8] showed in the stability analysis that 'Shear layers (with inflection point in the velocity profile) are unstable, but only for low frequencies; $f_{cav}\delta_0/u<1/4\pi$'. Fig.17 shows Nose 1 cases plotted in the Reynolds number based on the cavity depth Re_D versus $f_{cav}\delta/u$. For some cases of the cavity flow, as indicated in the figure, the laminar/turbulent condition is different from the far wake condition as explained in the correlation results of Fig.15. All cases are within the Hankey & Shang's unstable range ($f_{cav}\delta_0/u<1/4\pi$). And there seems to be an additional boundary: $Re_D\approx2750$, which divides unstable from stable for the cavity flow.

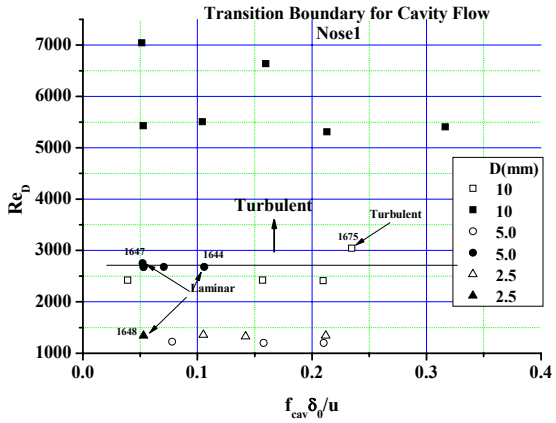

Fig.17 Transition Boundary Estimation for the Cavity Bottom Heating

Fig.17 also shows that the transition boundaries for far wake and inside cavity flow are very close each other except a very low Re_D case. This fact seems to show that the stability characteristics of the flow inside the cavity gives large influence on the cavity wake transition.

The constant value of Re_D for the cavity transition may show that the cavity transition seems to be related to the cavity vortex transition as the Re_D indicates the Reynolds number based on the cavity vortex core diameter. Further study will be necessary to clarify the transition within the cavity including the examination of different mechanisms of flow instability within the cavity such as the centrifugal instability of rear end corner vortex [17].

5 Conclusions

From a correlation study of the Mach 10 cavity wake heat transfer measurement test for various

geometry of cavities on the flat plate at an angle of attack of 35 degrees, following conclusions are obtained.

1) For the present experimental conditions, the St_m of the cavity wake peak, cavity far wake and cavity bottom surface heating with L/δ_0 and D/δ_0 correction correlated well with the estimated resonance frequency based on the closed-box acoustics models.

2) For the magnitude of cavity peak heating, correlation results showed a single correlation line. This result will show that the amount of wake peak heating may be caused by unstable shear layer reattachment that have enough oscillation magnitude to cause turbulent peak heating.

3) For the heating at the cavity far wake region and at the cavity bottom surface of the sharp nose model, the correlation showed two laminar and turbulent correlation lines. The transition of the cavity far wake and inside cavity flow may be mainly caused by the frequency and the amplitude of the shear layer instability oscillation.

4) For the blunt nose heat transfer correlation inside the cavity, the correlation results showed a single correlation line. This difference between the blunt nose and sharp nose may come from shear layer profile difference caused by the nose bluntness effect. Further study for the instability of the flow inside the compressible high Mach number cavity flow and cavity wake flow will be necessary, including its influence on the transition and heating mechanism.

References

[1] Rossiter, J. E. Wind-tunnel experiments on the flow over rectangular cavities at subsonic and transonic speeds. *Aeronautical Research Council Reports and Memo* No.3438, 1966.

[2] Heller, H.H Holmes, D.G and Covert, E.E. Flow-induced pressure oscillations in shallow cavities. *Journal of Sound and Vibration,* Vol.18, No.4, pp.545-553, 1971.

[3] Tam, C.K.W and Block, P.J.W. On the tones and pressure oscillations induced by flow over rectangular cavities. *J. Fluid Mech.*, 89, part 2, pp. 1978.

[4] Hozumi, K and Koyama, T. Heat conduction effect at strong local heating region in hypersonic heat flux measurement test," *The proceedings of 23rd ISTS, Matsue*, ISTS 2002-e-03, May 2002.

[5] Perry, A and Hornung, H. Some aspects of three-dimensional separation, Part II: Vortex skeletons. *Z. Flugwiss. Weltraumforsch.* 8, Heft 3, pp.155-160, 1984.

[6] Perry, A.E and Chong, M.S. A Description of eddying motions and flow patterns using critical-point concept. *Ann. Rev. Fluid Mech.* Vol.19, pp.125-155, 1987.

[7] Koyama, T Hozumi, K Tsuda, S Hirabayashi, N Sekine, H and Nagai, S. Aerodynamic heating measurement around cavities to estimate spaceplane TPS tile damage heating. *The 45th Space Sciences and Technology Conference*, Paper No.01-1B9, October 2001.(In Japanese.)

[8] Hankey, W.L and Shang, J.S. Analysis of pressure oscillations in an open cavity. *AIAA Journal*, Vol.18, No.8, pp.892- 898, August 1980.

[9] Takakura, Y Suzuki, T and Higashino, F. Numerical study on supersonic internal cavity flows: What causes the pressure fluctuations?. AIAA-99-0545, January 1999.

[10] Űnalmis, Ő.H Clemens, N.T and Dolling, D.S. Experimental study of shear-layer/acoustics coupling in Mach 5 cavity flow. *AIAA Journal*, Vol.39, No.2, pp.242-252, February 2001.

[11] Gropengiesser, H. On the stability of free shear layers in compressible flows. *Deutsche Luft, und Raumfahrt*, FB 69-25, 1969.

[12] Ragab, S.A and Wu, J.L. Linear instabilities in two dimensional compressible mixing layers. *Phys. Fluids A*, 1(6), pp.957- 966, 1989.

[13] Jackson, T.L and Grosch, C.E. Invicid special stability of a compressible mixing Layer. Part 3. Effect of thermodynamics. *J. Fluid Mech.*, 224, pp.159-175, 1991.

[14] Rowley, C.W Colonius, T and Basu, A.J. On self-sustained oscillations in two-dimensional compressible flow over rectangular cavities. *J. Fluid. Mech*. Vol.455, pp.315-346, 2002.

[15] Lam, J.P. Correlation of convective heat transfer for open cavities in supersonic flow. *AIAA Progress in Astronautics and Aeronautics: Aerothermodynamics and Planetary Entry*, Vol.77, AIAA, New York, pp.36-50, 1981.

[16] White, F. *Viscous fluid flow*. MaGraw-Hill Book Company, New York. pp.586-600. 1974.

[17] Albensoeder, S Kuhlmann, H.C and Rath, H.J. Three-dimensional centrifugal-flow instabilities in the lid-driven-cavity problem. *Physics of Fluids*, Vol.13, No.1, pp.121-135, January 2001.